molecules

MDPI

Article

Synthesis and Structural Investigation of New Bio-Relevant Complexes of Lanthanides with 5-Hydroxyflavone: DNA Binding and Protein Interaction Studies

Alexandra-Cristina Munteanu [1], Mihaela Badea [2], Rodica Olar [2], Luigi Silvestro [3], Constanţa Dulea [3], Constantin-Daniel Negut [4] and Valentina Uivarosi [1,*]

1 Department of General and Inorganic Chemistry, Faculty of Pharmacy, "Carol Davila" University of Medicine and Pharmacy, 6 Traian Vuia Str., 020956 Bucharest, Romania; alexandra.ticea@umf.ro
2 Department of Inorganic Chemistry, Faculty of Chemistry, University of Bucharest, 90-92 Panduri Str., 050663 Bucharest, Romania; e_m_badea@yahoo.com (M.B.); rodica_m_olar@yahoo.com (R.O.)
3 PharmaServ. International SRL, 52 Sabinelor Str., 050853 Bucharest, Romania; dreispharmasl@aol.com (L.S.); dulea_c@yahoo.com (C.D.)
4 Horia Hulubei National Institute of Physics and Nuclear Engineering (IFIN-HH), IRASM Radiation Processing Department, Reactorului Str. 30, 077125 Magurele-Ilfov, Romania; dnegut@nipne.ro
* Correspondence: uivarosi.valentina@umf.ro; Tel.: +40-740-593-237

Academic Editor: Arnaud Gautier
Received: 11 November 2016; Accepted: 13 December 2016; Published: 16 December 2016

Abstract: In the present work, we attempted to develop new metal coordination complexes of the natural flavonoid 5-hydroxyflavone with Sm(III), Eu(III), Gd(III), Tb(III). The resultant hydroxo complexes have been characterized by a variety of spectroscopic techniques, including fluorescence, FT-IR, UV-Vis, EPR and mass spectral studies. The general chemical formula of the complexes is $[Ln(C_{15}H_9O_3)_3(OH)_2(H_2O)_x]\cdot nH_2O$, where Ln is the lanthanide cation and x = 0 for Sm(III), x = 1 for Eu(III), Gd(III), Tb(III) and n = 0 for Sm(III), Gd(III), Tb(III), n = 1 for Eu(III), respectively. The proposed structures of the complexes were optimized by DFT calculations. Theoretical calculations and experimental determinations sustain the proposed structures of the hydroxo complexes, with two molecules of 5-hydroxyflavone acting as monoanionic bidentate chelate ligands. The interaction of the complexes with calf thymus DNA has been explored by fluorescence titration and UV-Vis absorption binding studies, and revealed that the synthesized complexes interact with DNA with binding constants (K_b) ~10^4. Human serum albumin (HSA) and transferrin (Tf) binding studies have also been performed by fluorescence titration techniques (fluorescence quenching studies, synchronous fluorescence spectra). The apparent association constants (K_a) and thermodynamic parameters have been calculated from the fluorescence quenching experiment at 299 K, 308 K, and 318 K. The quenching curves indicate that the complexes bind to HSA with smaller affinity than the ligand, but to Tf with higher binding affinities than the ligand.

Keywords: lanthanides; chelates; density functional calculations; calf thymus DNA; HSA; transferrin

1. Introduction

Flavonoids are among the most intensively studied and diverse class of plant metabolites. Animals and humans do not produce this group of phytochemicals, but consume them daily through food. Flavonoids can influence various cellular processes, including membrane transport, protein assembly, cell signal transduction, intracellular reduction-oxidation processes, and gene expression [1].

Due to the favorable spatial arrangement of the hydroxyketone moiety in their structures, flavonoids have been successfully used in coordination chemistry as ligands. Therefore, flavonoids

have the ability to bind metal ions in multiple oxidation states, forming stable coordination complexes [2]. The metal complexes thus formed show in many cases greater therapeutic potential than the parent ligand.

Lanthanide (Ln) coordination chemistry has registered substantial progress in the last two decades due to its numerous applications. Trivalent lanthanide cations behave as "hard" Lewis acids. Therefore, their affinities toward "hard" ligands with oxygen donor atoms, such as flavonoid derivatives, will be very strong [3]. The design of Ln complexes is focused on potential application in areas such as extraction and separation, catalysis, nonlinear optics (NLO), luminescent probes, magnetism, or is pointing towards therapeutic potential as antioxidant, anticancer [4–6], or antimicrobial agents [7]. Because of their long wavelength emission and lifetimes, Ln complexes have the potential for application as sensors and probes in biological and biomedical research [8].

Studies of the interaction between some lanthanide ions and flavonoid molecules led to the isolation and characterization of solid complexes derived from chrysin, $Ln(C_{15}H_9O_4)_3 \cdot 4H_2O$ (where: $C_{15}H_9O_4$ is deprotonated chrysin) [9], $[Ln(chrysin)_3]$ [10], $[LnL_2(H_2O)_2Cl]$ (L: chrysin) [11], quercetin, $[Ln(quercetin)_3] \cdot nH_2O$ [12], or morin, $Ln(morin)_3$ [13], $Ln(C_{15}H_9O_7)_3 \cdot nH_2O$, where n = 6 or 8, $C_{15}H_9O_7$ = morin [14,15].

Interactions of flavonoid metal complexes with DNA are well documented in literature, as they are relevant for the rational design of efficient antitumor and antimicrobial agents [16] or potential probes of DNA structure and conformation [17]. Ln-flavonoids complexes interact with DNA in a non-covalent way, mostly by intercalation between DNA base pairs or outside bonding. Intermolecular H-bonds and electrostatic forces may also be involved in the binding process [17–21]. The values of the binding constants vary between 10^2–10^7 M^{-1}.

Human serum albumin (HSA) is the most abundant extracellular protein of the circulatory system. Studies of drug-HSA interactions may bring valuable information regarding the pharmacokinetics of that substance, thus being useful for drug design and screening [22]. Transferrin (Tf) is involved in metal ions transportation throughout the organism (mainly iron) [23]. Cancer cells, as active and rapidly proliferating cells, express high levels of transferrin receptors. Consequently, transferrin is a potential drug carrier for targeted delivery into tumor cells [24]. To our knowledge, there are no reported studies on the interaction between Ln-flavonoid complexes and HSA or Tf. Primuletin (5-hydroxyflavone; 5-hydroxy-2-phenyl-4*H*-1-benzopyran-4-one, Figure 1) occurs naturally in *Primula* sp. [25] and *Dionisya* sp. [26]. In comparison to other flavonoids, the biological activity of 5-hydroxyflavone (5-HOF) is yet poorly explored. To date, it has been reported that 5-HOF acts as an agonist of calcium-activated and ATP-sensitive potassium channels [27], and has strong vasorelaxing and androgen receptor antagonistic activity [28].

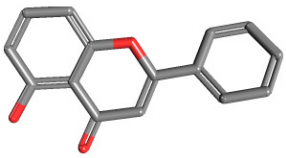

Figure 1. Primuletin (5-hydroxyflavone).

Due to the presence of a chelating 5-hydroxy-4-keto moiety, 5-hydroxyflavone can act as a bidentate ligand toward ions of *p*-, *d*-, and *f*-metals. Several metal complexes of 5-hydroxyflavone have been obtained in solution or synthesized in solid state [29–34]. However, their applications are limited: 5-hydroxyflavone-Al(III) complex has been designed as a fluorescent fluoride ion probe [33] and $[Be(5\text{-HOF})_2]$ has been tested as electroluminescent material in organic light-emitting diodes [34].

Our study aims to present the synthesis and structural characterization of four new solid complexes of 5-hydroxyflavone with some lanthanide ions: samarium(III), europium(III), gadolinium(III), and terbium(III). Studies regarding DNA- and protein-interactions have been performed in order to assess the potential biological applications of the complexes.

2. Results and Discussion

2.1. Synthesis

The complexes reported in this paper were obtained according to the general synthesis scheme depicted in Scheme 1.

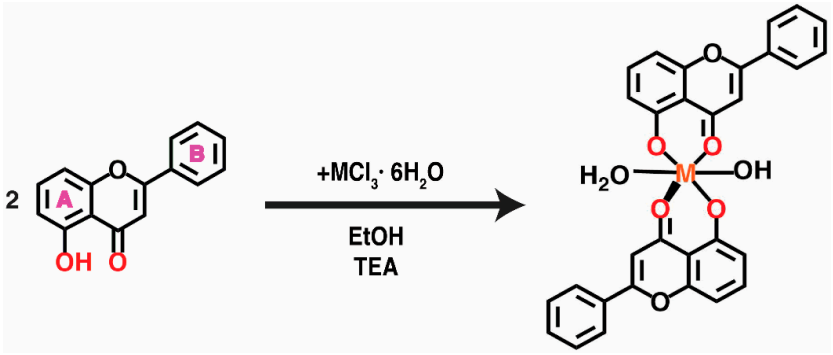

Scheme 1. The reaction scheme for the synthesis of complexes, where MCl_3 = the lanthanide salt, EtOH = ethanol, TEA = triethylamine.

The abbreviated formulas that we have attributed to the four complexes and that will be used in this work are as follows:

$[Sm(OH)L_2]$ (**1**)

$[Eu(OH)L_2(H_2O)]\cdot H_2O$ (**2**)

$[Gd(OH)L_2(H_2O)]$ (**3**)

$[Tb(OH)L_2(H_2O)]$ (**4**)

where

- L = $C_{15}H_9O_3$, deprotonated 5-hydroxyflavone
- The metal complexes were assigned the following codes, that will be used further in this article: (**1**), (**2**), (**3**), (**4**); 5-hydroxyflavone will be used as 5-HOF

Adding triethylamine assures the deprotonation of the ligand, so that 5-hydroxyflavone acts as a monoanionic bidentate chelate coordinated via 5-hydroxy-4-keto moiety.

2.2. Physicochemical Characterization

The colour of the prepared complexes is yellow. Complexes (**1**)–(**4**) have been found to be very soluble in DMF and DMSO and moderately soluble in chloroform. However, complex (**1**) is less soluble in DMSO than the other three complexes. Their solubility in ethanol, methanol, acetonitrile, acetone and water is very low. Low molar conductance values show that the complexes are non-electrolytes in DMSO.

2.2.1. IR Spectra

The spectra of the ligand and the complexes provide information about the coordination of Sm(III), Eu(III), Gd(III), and Tb(III) ions to 5-hydroxyflavone. The intense broad band between 2600 and 3200 cm^{-1} which appears in the IR spectra of 5-hydroxyflavone [35] is due to the the strong intramolecular hydrogen bond involving the phenolic hydroxyl in the free ligand. A sharp band at 3059 cm^{-1} corresponds to the stretching vibration ν(C-H). In the IR spectra of the complexes (except for (**1**)) a broad band between 2600 and 3600 cm^{-1} is found, assigned to the presence of water of hydration

in their structure. The intense absorption bands due to ν(C=O) in the free ligand, placed at 1654 and 1615 cm^{-1} appear shifted to lower frequencies in the spectra of the complexes. The displacement of ~20 cm^{-1} can be explained by the involvement of the carbonyl oxygen in metal binding. The strong band which appears at 1587 cm^{-1} in the IR spectrum of the ligand was assigned to ν(C=C). In the IR spectra of the complexes, this band is slightly shifted, indicating that this bond is not involved in coordination. In the IR spectrum of the ligand a strong band appears at 1298 cm^{-1}, assigned to the coupled vibration ν(C-O) + δ(OH). The same band appears very weak in the spectra of the complexes, which indicates that 5-hydroxyflavone is coordinated in its deprotonated form. The ν(C-O-C) frequency does not appear shifted in the spectra of the complexes, which confirms that the ring oxygen is not involved in coordination. Moreover, in the spectra of the complexes, the presence of ν(M-O) stretching vibration at ~560 cm^{-1} indicates metal binding, since the spectrum of the ligand does not exhibit this band [35,36].

2.2.2. UV-Vis-NIR Spectra

The ligand, 5-hydroxyflavone, exhibited two absorption maxima originated from π-π* transitions at 385 nm (band I) and 255 nm (band II). Band I is related to the transition localized within the B ring (cinnamoyl system), whereas band II is due to the transitions in the A ring (benzoyl system) [37,38] (the A and B ring are depicted in Scheme 1). Bathochromic shifts regarding these two bands are observed in the spectra of the complexes, which can be related to the extension of the conjugated system of the ligand with coordination [39]. The shoulder that appears at 340 nm in the electronic spectrum of the ligand, is also present in the electronic spectra of complexes as shoulder or maximum, with a hypsochromic shift (Δλ~20–25 nm). UV-Vis data for ligand and complexes are presented in Table S1. In the NIR region of spectrum, the characteristic f-f transitions form the ground state $^6H_{5/2}$ to ^6F multiplet of Sm^{3+} ion ($4f^5$) are observed (Figure 2) [40].

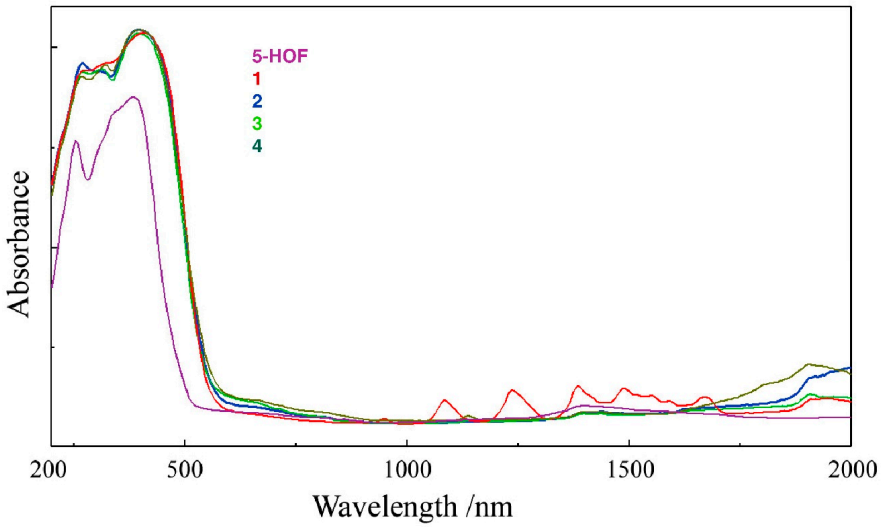

Figure 2. Electronic spectra of the ligand and the complexes (recorded on solid probes).

2.2.3. Mass Spectra

The compounds analysed gave intense pseudomolecular ions by protonation as well as adducts with one or two water molecules ions (Table S2 columns 2nd, 3rd, 4th); for all products the spectra were in agreement with the natural isotopic abundances of the lanthanides involved. Protonated pseudomolecular ions of all compounds, with the exception of that with Sm(III) formed, by collision with nitrogen, intense fragment ions corresponding to the loss of a ligand molecule (Table S2, 5th column). All data obtained by mass spectrometry confirm that these compounds have a 1:2 molar ratio metal ion: ligand (Figure S1).

2.2.4. Thermal Behavior

Thermal analysis is frequently used in order to obtain useful information concerning both the composition and stability of the complexes. As a result, the thermal behaviour of the four new lanthanide complexes was investigated in air by simultaneous TG/DTA analysis. The thermal decomposition data are summarized in Table 1 and will be discussed as follows.

Table 1. Thermal decomposition data (in air flow) for complexes (**1**)–(**4**).

Complex	Step	Thermal Effect	Temperature Range (°C)	Δm_{exp} (%)	Δm_{calc} (%)
(**1**)	1	Exothermic	320–1000	72.5	72.8
		Residue (Sm_2O_3)		27.5	27.2
(**2**)	1	Endothermic	170–300	5.0	5.3
	2	Exothermic	320–1000	72.2	72.3
		Residue (Eu_2O_3)		22.8	22.4
(**3**)	1	Endothermic	240–315	2.6	2.7
	2	Exothermic	325–1000	69.9	70.1
		Residue (Gd_2O_3)		27.5	27.2
(**4**)	1	Endothermic	210–310	2.5	2.7
	2	Exothermic	320–1000	69.6	69.9
		Residue (Tb_2O_3)		27.9	27.4

The TG, DTG and DTA curves registered for Sm(III) complex (**1**) are shown in Figure S2 and indicate that this compound is anhydrous and stable up to 320 °C and then undergoes oxidative degradation of the organic part.

For the other three complexes, (**2**)–(**4**), the thermal decomposition curves are quite similar, consisting in water molecules elimination and oxidative degradation of organic ligands. For the europium complex which possesses both coordination and crystallization water molecules the thermal decomposition starts at 170 °C, this being the lowest decomposition starting temperature. All anhydrous species are stable up to 320 °C.

In the final step the organic part oxidative degradation occurs, accompanied by several overlapped exothermic processes as can be noticed on DTA curve. All these processes lead to the most stable species M_2O_3 as final products.

In conclusion, according to DTG and DTA curves, the thermal transformations are complex processes consisting in water (crystallization or coordination) elimination, thermolysis and oxidative degradation of 5-hydroxyflavone (Figure S2).

2.2.5. Fluorescent Properties

The fluorescence emission spectra (Figures S3 and S4) were recorded in chloroform at a concentration of 5 μg/mL at the excitation wavelengths of 360 nm and 440, respectively, both for ligand and complexes. The results let us draw the following conclusions:

(i) 5-hydroxyflavone does not exhibit fluorescence in the stated conditions;
(ii) at the excitation wavelength of 360 nm, two new bands appeared at 411 and 436 nm in the fluorescence emission spectra of the complexes (**1**) and (**2**).
(iii) At the excitation wavelength of 440 nm, a new band appeared at 481 nm in the fluorescence emission spectra of complex **1**.

The new bands that appeared in the emission spectra of complexes could be appreciated as evidence for the formation of a chelate ring via coordination of the metal ion, which increases the rigidity of the ligand structure and enhances the fluorescence quantum yield by reducing the probability of non-radiative dissipation process.

2.2.6. EPR Spectroscopy

Gd^{3+} ions, with a $4f^7$ electronic configuration, have a larger relaxation time (10^{-9}–10^{-10} s) [41], exhibiting detectable EPR signals at room temperature. Tb(III) and Eu(III) ions, due to their short relaxation times (10^{-13} s), do not normally show EPR signals at room temperature [42].

Figure 3 shows the solid state EPR spectrum of **3**, recorded at room temperature. The spectrum is dominated by a very broad, slightly asymmetrical line (marked by g_1 in the figure) with an effective g factor of 1.99 and the peak-to-peak linewidth (ΔB_{pp}) of about 175.5 mT. Additionally, a weak, unresolved resonance (g_2) can be observed at g = 3.47, with a $\Delta B_{pp} \approx 29.17$ mT. The resonance at $g \sim 2.0$ is typical for Gd(III) located in low-symmetry sites [43]. The paucity of fine structure and line broadening indicate a week crystal field [44].

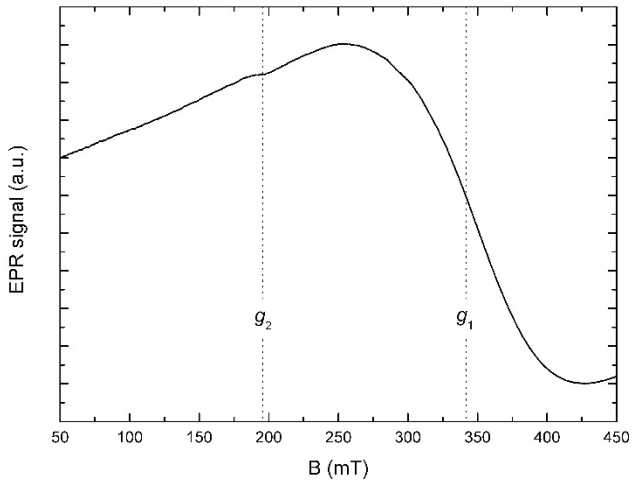

Figure 3. EPR spectrum of **3** (powder) recorded at room temperature.

2.3. DFT Calculations

The fully optimized geometries of the ligand and complexes **1**–**4** and the symbols and the labels of atoms are shown in Figures 4 and 5.

The B3LYP functional is used frequently and provides good results. We have used the unrestricted version, uB3LYP. The optimizations were employed under no symmetry restrictions and vibrational frequencies were additionally calculated at the same level of theory in order to confirm that the optimized structures are true minima (with no imaginary frequencies).

Selected bond lengths, angles, charge density, total energy and total dipole moment are presented in Tables 2 and 3.

The coordination sphere around the metal centre in complex (**1**) (Figure 4) is made up of the following atoms: O7, O27 and O29, O30 (belonging to 5-hydroxyflavone) and O31 (belonging to the hydroxyl group). The coordination sphere around the metal centre in complexes (**2**)–(**4**) has one extra O atom, belonging to a water molecule.

In complexes (**2**)–(**4**), the O-M-O bond angles in the complexes vary between 46°–106° which indicate a distorted octahedral geometry. The values of the dihedral angles around the lanthanide ion in complexes (**2**)–(**4**) (Figure 5), are far from 0° or 180° which indicate that the lanthanide ion and the donating sites do not lie in the same plane. In complex (**1**), the corresponding dihedral angles are close to 0° (−1.366°) and 180° (179.599°), indicating that Sm^{3+} is situated in the same plane with the moieties involved in coordination [45].

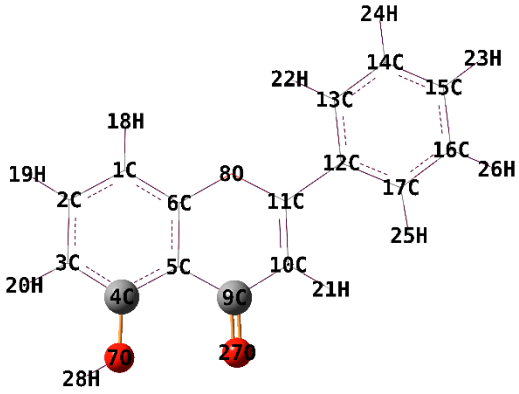

Figure 4. The optimised structure of the electronic ground state of 5-hydroxyflavone at the B3LYP level of theory (6-31G(d) basis).

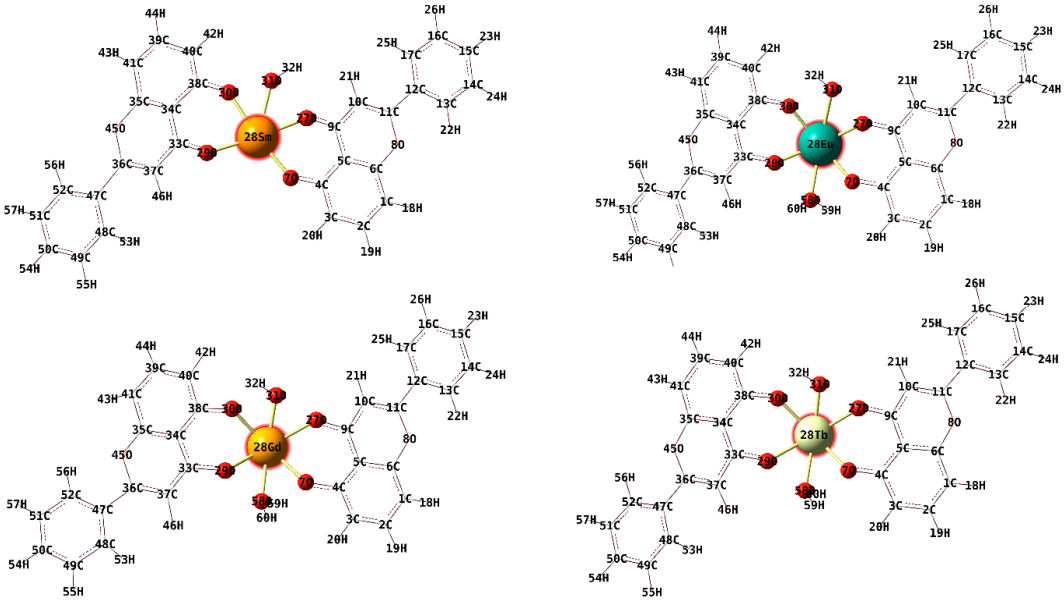

Figure 5. The optimised structure of the electronic ground state of complexes (**1**)–(**4**) at the uB3LYP level of theory (6-31G(d) basis set for C, H atoms; 6-31G+(d,p) for O atoms; MWB28 for lanthanide atoms).

Table 2. Geometric parameters bond lengths (A), bond angles (°), charge density, total energy (a.u.) and total dipole moment (D) of 5-hydroxyflavone as resulted from DFT calculations.

Bond Length (A)			
C4-O7	1.351		
C9=O27	1.221		
Bond Angle (°)			
C4-C5-C9	122.998		
O7-C4-C5	120.781		
O27-C9-C5	121.151		
Charge			
C4	0.836	O7	−0.434
C9	0.448	O27	−0.469
Total energy (a.u.)		−802.4868	
Total dipole moment (D)		4.3673	

Table 3. Geometric parameters bond lengths (A), angles (°), charge density, total energy and total dipole moment of complexes (**1**)–(**4**) as resulted from DFT calculations.

Parameter	Complex			
	(1)	**(2)**	**(3)**	**(4)**
Bond Length (A)				
M-O7	2.155	2.149	2.156	2.150
M-O27	2.132	2.120	2.233	2.201
M-O29	2.167	2.151	2.252	2.259
M-O30	2.149	2.146	2.177	2.124
M-O31	2.361	2.485	2.395	2.395
M-O58	-	2.410	2.379	2.378
C9-O27	1.276	1.304	1.306	1.307
C4-O7	1.281	1.312	1.310	1.315
Bond Angle (°)				
O27-M-O31	54.577	48.731	51.462	51.624
O27-M-O7	73.051	71.572	71.167	71.512
O7-M-O29	111.091	105.489	97.734	97.707
O30-M-O31	46.376	49.686	53.136	50.077
O30-M-O29	74.919	71.119	69.736	72.046
O29-M-O58	-	57.411	48.829	49.279
O58-M-O7	-	50.274	51.109	50.623
C4-C5-C9	122.998	120.776	119.586	121.189
O7-C4-C5	120.781	120.263	121.871	120.425
Dihedral Angle				
M-O27-C9-C5	−1.366	−21.069	−30.917	−30.948
M-O7-C4-C5	−3.011	18.903	18.397	18.769
O31-M-O7-C4	−1.855	−41.144	−47.061	−47.380
M-O7-C4-C3	179.599	−158.486	−156.593	−156.435
M-O29-C33-C37	164.413	136.736	139.683	145.150
Charge				
M	1.079	1.186	0.887	1.076
O7	−0.705	−0.585	−0.541	−0.556
O27	−0.611	−0.377	−0.395	−0.344
O29	−0.639	−0.468	−0.383	−0.396
O30	−0.568	−0.529	−0.592	−0.556
O31	−0.501	−0.521	−0.416	−0.549
O58	–	−0.635	−0.626	−0.628
C4	0.406	0.228	0.221	0.213
C9	0.561	0.206	0.163	0.121
C33	0.554	0.255	0.141	0.162
C38	0.406	0.221	0.281	0.233
Total energy (a.u.)	−1706.6004	−2467.6373	−2522.8014	−2581.6789
Total dipole moment (D)	4.3164	7.2773	6.7800	5.6414

2.4. In Vitro Interactions with Biological Macromolecules

2.4.1. DNA Binding Studies

Drugs bind to DNA both covalently (irreversibly) and non-covalently (reversibly). Covalent binding to DNA often leads to complete inhibition of vital processes and subsequent cell death. Reversible binding with double-stranded DNA mainly follows three patterns: the drug molecules interact: (*i*) with the external negatively charged nucleic sugar-phosphate structure, via electrostatic binding; (*ii*) with the minor and/or major grooves of DNA double helix-usually implies electrostatic forces, van der Waals interactions, hydrogen bonds, dative bonds and/or hydrophobic interactions; or (*iii*) the

drug molecules intercalate between DNA base pairs (the DNA-drug complex is stabilized by the π-π* stacking interactions between the aromatic systems of the tested compound and DNA bases). Intercalators are usually planar heterocyclic compounds which stack between adjacent base pairs in the DNA structure. Flavonoids and their metal complexes possess such planar structures due to the conjugated π-bond ring system, and, therefore, have the potential to intercalate between DNA bases and to form stable complexes. Several studies revealed that the above mentioned compounds bind to DNA via groove interactions or intercalation [46,47].

UV-Vis Spectroscopy Studies

In order to explore the mechanism of DNA-Ln(III) complexes interaction, the spectrophotometric titration of the complexes in the presence of highly polymerized CT-DNA was performed. We evaluated the changes in the recorded spectra, like hypsochromic (blue-shift), bathochromic (red-shift) or hypochromic effects, commonly considered as evidence of DNA-drug interactions [48].

Binding in a nonintercalative manner with DNA, generally results in hyperchromism due to the strong disturbances induced in the DNA double helical structure. Nonetheless, intercalation generally results in hypochromism and red shift due to strong π-π* stacking interactions between an aromatic moiety of the ligand and DNA nucleotides.

In the UV spectra of the three complexes after the addition of increasing DNA concentrations, the band centered at ~273 nm exhibits a significant hypochromism of ~40% (Figure 6 and Figure S5), suggesting strong binding to CT DNA, possibly by intercalation [49]. Furthermore, in regard to spectral general features, a strong resemblance of the four compounds can be noticed, therefore similar binding modes to CT-DNA are expected. Complex (**1**) was also tested in the same conditions, but the results did not follow any recognizable pattern of interaction with CT-DNA, if any.

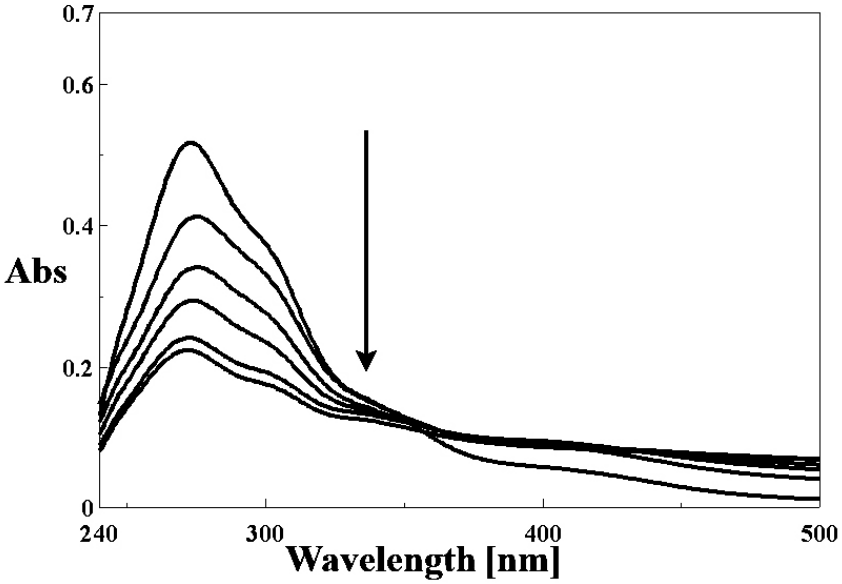

Figure 6. Absorption spectra of complex **2** in the absence and presence of increasing amounts of DNA, respectively; [complex] = 15 μM; [DNA] = 0; 5; 10; 15; 25; 30 μM. The arrow shows the absorption changes on increasing DNA concentration.

The following equation has been used to calculate the binding constant of 5-hydroxyflavone and its Ln(III) complexes [22]:

$$\frac{A_0}{A - A_0} = \frac{\varepsilon_c}{\varepsilon_{DNA-c} - \varepsilon_c} - \frac{\varepsilon_c}{\varepsilon_{DNA-c} - \varepsilon_c} \times \frac{1}{K[Q]},$$

where A_0 and A represent the absorbance of DNA in the absence and presence of the ligand and the complexes (**2**), (**3**), (**4**) at λ_{max} = 258 nm, ε_c and ε_{DNA-c} are the absorption coefficients of the tested compounds and compound-DNA system, respectively. The plot of $A_0/(A - A_0)$ vs. 1/[Q] is constructed by using the absorption titration data and linear fitting (Figure 7 and Figure S6). The calculated binding constants for 5-HOF and complexes (**2**), (**3**), (**4**), respectively are presented in Table 4.

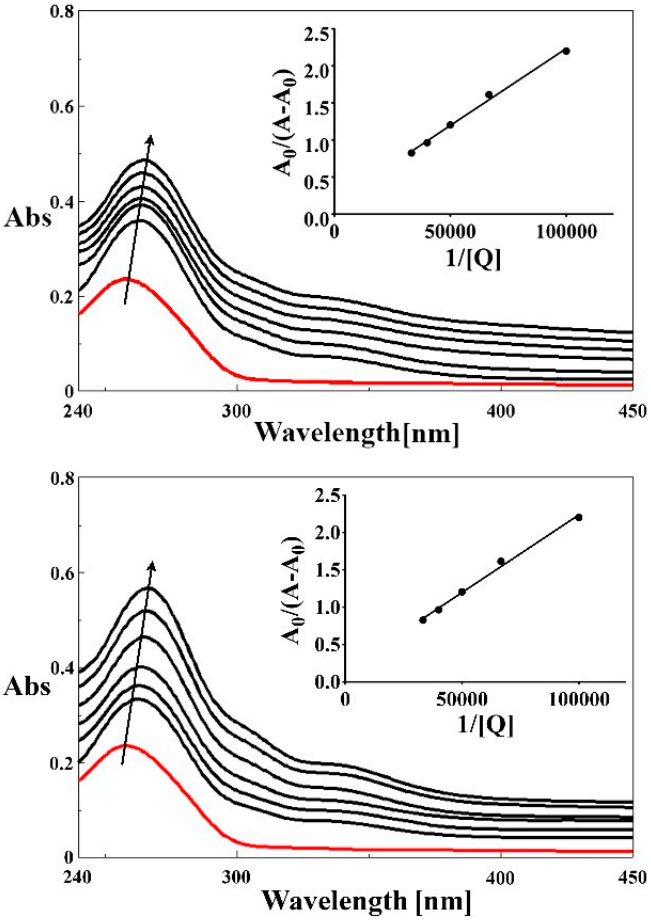

Figure 7. Absorption spectra of DNA in the absence and presence of increasing amounts of 5-HOF and complex (**2**). [DNA] = 15 μM; [compound] = 0; 5; 10; 15; 20; 25; 30 μM. Insert figures represent the plots of $A_0/(A - A_0)$ vs. 1/[Q]. The arrows show the absorption changes on increasing concentration of the tested compound.

Table 4. Binding constants for 5-HOF and complexes (**2**), (**3**), (**4**), respectively and CT-DNA interaction systems.

Compound	K_b ($L \cdot mol^{-1}$)	R^2
5-HOF	1.47×10^4	0.9999
(**2**)	2.73×10^4	0.994
(**3**)	2.93×10^4	0.9934
(**4**)	3.85×10^4	0.9981

Moreover, as comparing to ethidium bromide (EB), which is a classical intercalator, with a K_b ~10^5 M^{-1}, these values are not much smaller. Interaction of the four compounds with CT-DNA is weaker than the DNA interaction with typical intercalators. However, an electrostatic and/or intercalative interaction may explain EB displacement from the EB-DNA complex.

Competitive Binding Studies with Ethidium Bromide Using Fluorescence Spectroscopy

Ethidium bromide (3,8-diamino-5-ethyl-6-phenylphenanthridinium bromide, EB) is a fluorescent dye, which has a planar phenanthridinium ring in its structure. Due to the intercalation of this planar ring between adjacent base pairs on the DNA double helix, EB emits intense fluorescence in the presence of CT DNA, after the formation of an EB-DNA complex. Therefore, an EB-bound CT-DNA solution (2 μM EB + 10 μM DNA) has been used as a spectral probe.

When the metal complexes bind to DNA, a decrease in the emission intensity of the EB-DNA complex is recorded (a quenching effect). The variation of the fluorescence emission intensity gives some information about the DNA binding affinity of the metal complexes and usually indicates the existence of stacking interactions (intercalation) between the DNA base pairs.

Data from the competitive binding studies have been plotted according to the classical Stern–Volmer equation [50]:

$$I_0/I = 1 + K_{sv}\cdot[Q],$$

where I_0 and I represent the fluorescence intensities in the absence and presence of the compound respectively, and [Q] is the concentration of the tested compound.

The Ksv value is calculated as the slope of I_0/I versus [Q] linear regression plot (Table 5). The emission spectra of EB-DNA complex in the absence and presence of increasing concentrations of the ligand and complexes (**2**)–(**4**) are shown in Figure 8 and Figure S7. The quenching curves indicate that the complexes bind to CT-DNA with higher binding affinities than the ligand, in the order: 5-HOF < (**4**) < (**2**) < (**3**).

A small red shift (~5 nm) appears in the fluorescence spectra of EB-DNA upon binding to the tested compounds, due to the induced changes in the bond lengths and angles in the structure of the ligand (Figure 8).

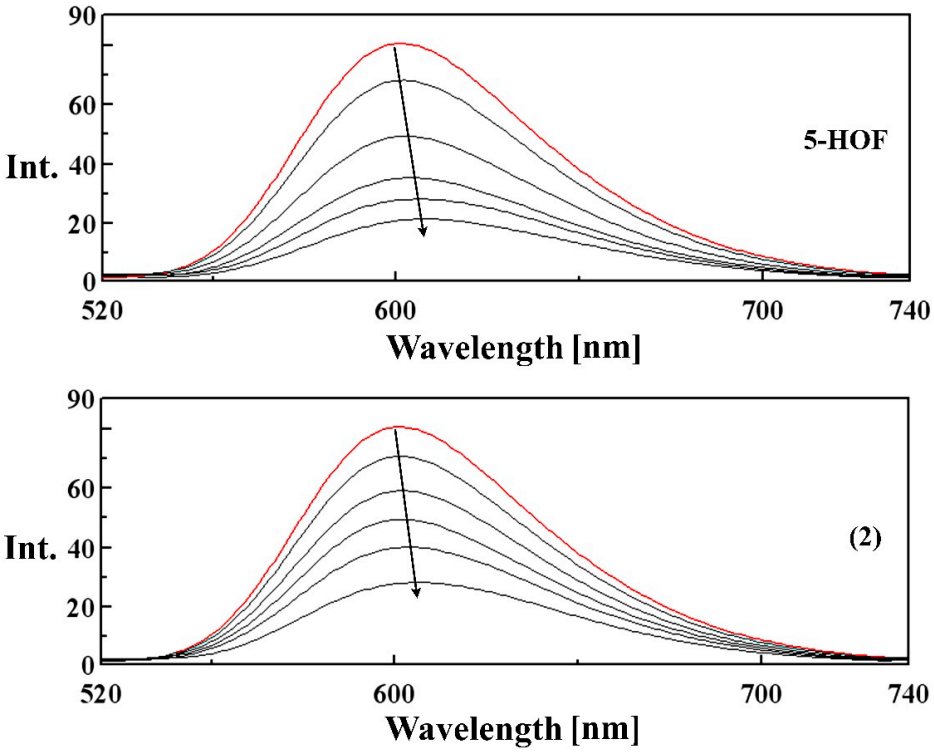

Figure 8. Fluorescence spectra of the binding of ethidium bromide (EB) to DNA in the absence (red line) and in the presence (black lines) of increasing amounts of the ligand and complex (**2**) λex = 500 nm, [EB] = 2 μM, [DNA] = 10 μM, [compound] = 10, 15, 20, 25, 30 μM. Arrows indicate the changes in fluorescence intensities upon increasing the amounts of the tested compound.

Table 5. Quenching constants of the interaction between the tested compounds and CT-DNA-EB complex.

Compound	K_{sv} (L·mol^{-1})	R^2
5-HOF	2.89×10^4	0.9928
(**2**)	1.73×10^5	0.9959
(**3**)	4.13×10^5	0.9941
(**4**)	1.39×10^5	0.9902

2.4.2. HSA and Tf Binding Studies

Insights into the nature of binding can be obtained from fluorescence quenching studies by monitoring the fluorescence intensities. Fluorescence spectroscopy is an effective method to explore the interactions of small molecules with proteins, such as HSA and Tf, which contain tryptophan residues. Variations of the fluorescence intensity of the chromophore may reflect changes in the microenvironment surrounding the fluorophore.

Fluorescence Quenching Mechanism

HSA exhibits a strong fluorescence emission peak at ~340 nm (when λ_{exc} = 280 nm) owing to the Tryptophan (Trp)-214 residue. The fluorescence intensity of Trp-214 may change when HSA interacts with other molecules. The quenching effect of 5-HOF and compounds (**1**)–(**4**) on the fluorescence intensity of HSA at 299, 308, 318 K are shown in Figures S8–S10, respectively. Trp, tyrosine (Tyr) and phenylalanine (Phe) amino acid residues in Tf have intrinsic fluorescence depending on the excitation wavelength. However, with fluorescence excitation at 295 nm, the tryptophan emission fluorescence is highly dominant [51]. The quenching effect of 5-HOF and compounds (**1**)–(**4**) on the fluorescence intensity of Tf at 299, 308, 318 K are shown in Figures S11–S13, respectively.

The intensity of the broad emission band decreased upon addition of increasing concentrations of the five tested compounds; the maximum emission wavelength of HSA exhibits a hypsochromic shift of up to 9 nm. This blue-shift effect indicates that the microenvironment around the tryptophan residue was disturbed, that the Trp residue is located in a more hydrophobic environment, becoming less exposed to the solvent [52]. On the other hand, the maximum emission wavelength of Tf does not appear shifted.

A modified Stern–Volmer equation was applied to the HSA and Tf fluorescence quenching data [23]:

$$\frac{F_0}{F_0 - F} = \frac{1}{f_a K_{sv}[Q]} + \frac{1}{f_a}$$

where F_0 and F are the relative fluorescence intensities of HSA and Tf, respectively, in the absence and presence of our tested compounds, respectively, f_a is the fraction of fluorophore accessible to the quencher, [Q] is the concentration of the quencher, and K_{SV} is the Stern–Volmer quenching constant. The resulted curves, depicted in Figures S14 and S15 show good linear relationships. Therefore, parameters K_a and f_a were calculated from the slope and intercept, respectively, in the plot of $F_0/(F_0 - F)$ vs. $1/[Q]$.

$$K_{sv} = K_q \tau_0,$$

where K_q is the bimolecular quenching rate constant and τ_0 is the lifetime of the fluorophore in the absence of the quencher.

The Stern–Volmer quenching constant (K_{SV}, M^{-1}) and the quenching rate constant (K_q, M^{-1} s^{-1}) for the ligand and the complexes which resulted from our studies are given in Table S3 (HSA) and Table S4 (Tf). These values suggest good binding affinity of the complexes with HSA and Tf. K_q values (>10^{11} M^{-1} s^{-1}) indicate the existence of a static quenching mechanism [53].

The following equation was used to determine K_a and n, where n is the number of binding sites [54]:

$$\lg\frac{F_0 - F}{F} = \lg K_A + n\lg[Q]$$

Plots of $\lg[(F_0 - F)/F]$ vs. lg[Q] for HSA and Tf-tested compounds systems 5-HOF, (**1**)–(**4**)) are represented in Figures S16 and S17. Temperature did not vary in a broad range, therefore the value of the enthalpy change could be considered to be constant and the van't Hoff equation can be used in order to estimate the thermodynamic parameters:

$$\ln K = -\Delta H/RT + \Delta S/R$$

where K is the binding constant at the corresponding temperature (K), ΔH is the enthalpy change, R is the gas constant and ΔS is the entropy change. The values of ΔH and ΔS were obtained from the slope and the y intercept of a lnK vs. 1/T. Moreover, the free energy change (ΔG) can be calculated from the following relationship:

$$\Delta G = \Delta H - T\Delta S$$

The negative values of ΔG presented in Tables S3 and S4 indicate that the HSA and Tf binding processes are spontaneous. Moreover, since both ΔH and ΔS values are negative for all the tested compounds, hydrogen bonds or van der Waals forces most probably play important roles in the compound-proteins interactions [55].

Changes of Tf Conformation Induced by the Interaction with the Tested Compounds

Conformational changes of a protein in terms of secondary or tertiary structures can be altered upon binding to small molecules. Synchronous fluorescence spectra bring information about the molecular surroundings of proteins. One major advantage of this method compared to conventional emission spectra is that even small variations in the absorption and/or emission bands affect the corresponding band in a synchronous spectrum much more than in the case of a conventional emission spectrum. This improves spectral resolution, thus facilitating the analysis of minor structural perturbations. Therefore, we have used synchronous scan fluorescence spectroscopy in order to verify the change of the structure of Tf when binding to our compounds, in the presence of increasing concentrations of our complexes and the ligand [55–57].

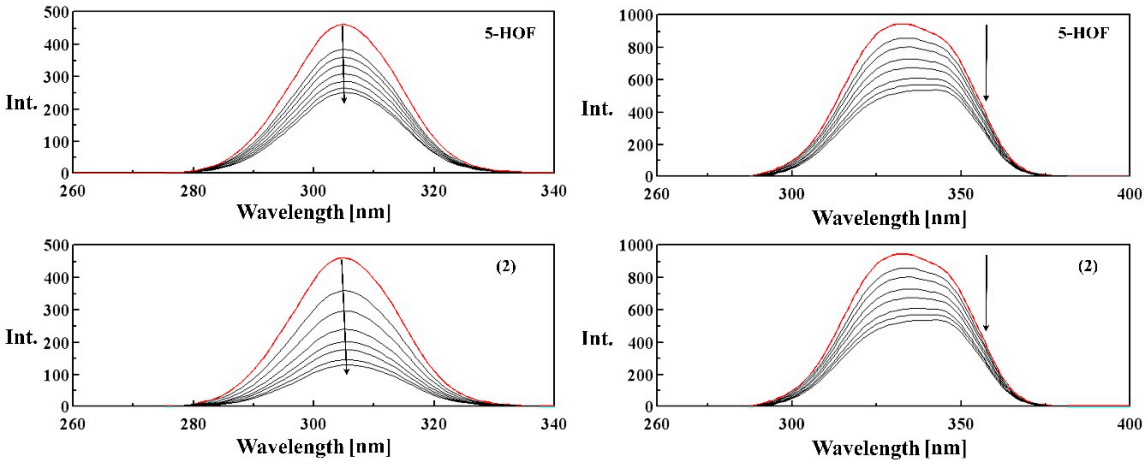

Figure 9. Fluorescence synchronous spectra of 5-HOF and complex (**2**) at Δλ = 15 nm (**left**) and 60 nm (**right**). [Tf] = 10 μM, pH = 7.4; [tested compound] = 0; 5; 7.5; 10; 12.5; 15; 17.5; 20 μM. Arrows indicate the changes in fluorescence intensities upon increasing the amounts of the tested compound.

Synchronous fluorescence spectra offer the characteristics of the tyrosine and tryptophan residues of transferrin when the wavelength interval ($\Delta\lambda$) between excitation and emission is 15 nm or 60 nm. Figure 9 and Figure S18 show the synchronous spectra of Tf in the absence and presence of different concentrations of our tested compounds. We have noticed that the emission maximum of tyrosine does not shift, whereas there was a red shift (up to 12 nm) of tryptophan residues fluorescence upon addition of the tested compounds. This indicates that the conformation of Tf around the tryptophan residues had changed, the polarity around this region had increased and the hydrophobicity had decreased [56].

3. Materials and Methods

3.1. Materials

All reagents and solvents were of analytical reagent grade and were used without further purification. 5-hydroxyflavone, $SmCl_3 \cdot 6H_2O$, $EuCl_3 \cdot 6H_2O$, $GdCl_3 \cdot 6H_2O$ and $TbCl_3 \cdot 6H_2O$, human transferrin and human serum albumin and double-stranded calf-thymus DNA were purchased from Sigma Aldrich Chemical Co. (Schnelldorf, Germany). All other chemicals and solvents were commercially available, and used without further purification.

3.2. Analytical Methods

Elemental analyses (for C, H, N, S) were performed using a PE 2400 analyser (Perkin Elmer, Billerica, MA, USA). The conductivity was measured with a Consort C830 (Turnhout, Belgium) conductimeter with an SK10T platinum electrode embedded in glass (cell constant 1.0 cm^{-1}). IR spectra were recorded using KBr pellets on a FT-IR VERTEX 70 spectrometer (Bruker, Billerica, MA, USA) in the range 400–4000 cm^{-1}. Electronic spectra by the diffuse reflectance technique, with spectralon as reference sample, were recorded in the range 200–2000 nm, on a V 670 spectrophotometer (Jasco, Tokyo, Japan). Fluorescence spectra were recorded on a Jasco FP 6500 spectrofluorometer.

Mass spectra were recorded, in positive mode scanning over a range m/z 100–1000, with an API 5000 (SCIEX-Canada, Concord, ON, Canada) triple quadrupole mass spectrometer equipped with a pneumatically assisted electrospray (ESI) source (Turbo spray model from SCIEX). Samples were dissolved in methanol at 10 $\mu g \cdot mL^{-1}$ and infused in the ESI source at 7 $\mu L \cdot min^{-1}$. Collision spectra (MS/MS), from protonated pseudomolecular ions, were acquired on the same instrument employing nitrogen as collision gas.

The heating curves (TG, DTG and DTA) were recorded using a Labsys 1200 SETARAM instrument (Setaram, Caluire, France) with a sample weight between 10 and 14 mg over the temperature range of 30–1000 °C and a heating rate of 10 $°C \cdot min^{-1}$. The measurements were carried out in synthetic air atmosphere (flow rate 17 $mL \cdot min^{-1}$), using alumina crucible. Sample masses were weighed on a microbalance with a resolution of 0.1 mg.

EPR measurements were carried out by means of a continuous-wave X-band spectrometer (MiniScope MS200, Magnettech, Berlin, Germany) equipped with a H102 rectangular resonator and 100 kHz modulation frequency. The spectrum was recorded at room temperature (24–26 °C) using a microwave power of 10 mW with modulation field amplitude of 0.2 mT.

3.3. Synthesis and Characterization of Complexes

Synthesis of complexes was carried out using the following general procedure: in a round bottomed flask provided with an electromagnetic stirrer, an ethanolic solution (25 mL) of 5-hydroxyflavone (1 mmol, 0.238 g), deprotonated with triethylamine (1 mmol, 140 µL) was added to an ethanolic solution (5 mL) of lanthanide chlorides (0.5 mmol). The reaction mixture was refluxed for 3 h. The yellow products formed were filtered off, washed several times with small amounts of a hot mixture of ethanol:water (1:1, v/v), and dried in an exsicator. The reaction scheme is shown in Scheme 1.

Complex (**1**)—Element. anal. found (calc.) $SmC_{30}H_{19}O_7$: %C 55.93 (56.14) and %H 2.67 (2.98); Molar conductance ($\Omega^{-1}\cdot cm^2\cdot mol^{-1}$): 5.8; IR $\overline{\nu}$ (cm^{-1}): 1636 (C=O); 1594 (C=O); 1343 (C-O + O-H); 1251 (C-O-C); 560 (Sm-O).

Complex (**2**)—Element. anal. found (calc.) $EuC_{30}H_{23}O_9$: %C 52.83 (53.03) and %H 3.32 (3.41); Molar conductance ($\Omega^{-1}\cdot cm^2\cdot mol^{-1}$): 5.6; IR $\overline{\nu}$ (cm^{-1}): 3600–2600 (broad band, O-H); 1637 (C=O); 1594 (C=O); 1581 (C=C); 1357 (C-O + O-H); 1252 (C-O-C); 562 (Eu-O).

Complex (**3**)—Element. anal. found (calc.) $GdC_{30}H_{21}O_8$: %C 54.18 (54.04) and %H 2.89 (3.17); Molar conductance ($\Omega^{-1}\cdot cm^2\cdot mol^{-1}$): 4.3; IR $\overline{\nu}$ (cm^{-1}): 3600–2600 (broad band, O-H); 1637 (C=O); 1595 (C=O); 1582 (C=C); 1358 (C-O + O-H); 1252 (C-O-C); 562 (Gd-O).

Complex (**4**)—Element. anal. found (calc.) $TbC_{30}H_{21}O_8$: %C 53.63 (53.90) and %H 2.82 (3.16); Molar conductance ($\Omega^{-1}\cdot cm^2\cdot mol^{-1}$): 5.1; IR $\overline{\nu}$ (cm^{-1}): 3600–2600 (broad band, O-H); 1637 (C=O); 1594 (C=O); 1581 (C=C); 1357 (C-O + O-H); 1252 (C-O-C); 563 (Tb-O).

3.4. Computational Study

Full geometry optimizations of the ligand and complexes were carried out using the DFT method in Gaussian09 [58]. The split valence double-zeta plus polarization basis set 6-31G(d) was applied for the carbon and hydrogen atoms. To give a better description of the lanthanide–ligand interactions, basis sets with additional diffuse functions were added for the oxygen atoms (6-31G+(d,p)). The Stuttgart-Cologne small-core quasi-relativistic pseudopotential ECP28MWB (28 electrons in the core) [59,60] was used for the Ln^{3+} ions. This ECP was used in combination with the optimized basis set: (14s13p10d8f6g)/[10s8p5d4f3g] [61]. DFT/B3LYP/(MWB28 for Ln^{3+}) was proven to give good results for prediction of coordination polyhedral and geometry parameters of metal complexes in other studies [62,63].

3.5. DNA Binding Studies

All experiments were performed in Tris-HCl buffer [tris(hydroxymethyl)aminomethane], containing 5 mM Tris-HCl and 50 mM NaCl, adjusted to pH 7.4. The concentration of the DNA solution was determined by measuring the absorption intensity at 260 nm, using the molar extinction coefficient value of 6600 $M^{-1}\cdot cm^{-1}$. The absorbances registered at 260 nm and 280 nm gave the ratios of ~1.8–1.9, indicating that the CT-DNA solution was sufficiently free of protein. Electronic absorption spectra were performed on a Jasco V 650 spectrophotometer using 1 cm quartz cuvettes at room temperature. Absorption titrations were determined in the range of 200–500 nm. We measured the absorbances of mixtures, containing constant concentrations of the tested complexes of 15 μM and increasing concentrations of the nucleic acid. We also measured the absorbances of mixtures, containing constant concentrations of CT-DNA (15 μM) and increasing concentrations of the tested compounds: 5, 10, 15, 20, 25, 30 μM. Each sample was kept for 10 min at room temperature to equilibrium before recording its spectrum.

Fluorescence spectra were recorded on a Jasco FP 6500 spectrofluorometer at room temperature. A sample containing CT-DNA (10 μM) and EB (2 μM) was titrated with concentrated solutions containing the tested compounds. For every addition, the mixture was shaken and kept for 10 min at room temperature, and then the fluorescence emission spectra were recorded. The experiments have been performed in Tris-HCl/NaCl buffer (pH 7.4, 5 mM Tris-HCl/50 mM NaCl). Fluorescence emission spectra were recorded with excitation at 500 nm in the range 520–740 nm.

3.6. Protein Binding Studies

Fluorescence measurements were performed on a Jasco FP 6500 spectrofluorometer in a 1 cm path-length quartz cell by fluorimetric titration. A 3.0 mL sample containing 10 μM HSA was titrated by successive additions of the ligand and the complexes (ranging from 0–25 μM, with an increment

of 2.5 μM). Each sample solution was shaken and kept for 3 min at the corresponding temperatures (299 K, 308 K and 318 K). The same procedure was used for Tf binding studies. Afterwards, the fluorescence spectra were recorded with the excitation wavelength set at 280 (for HSA) and 295 (for Tf) and the emission wavelength set at 290–500 nm (HSA) and 305–450 (Tf), respectively. In the meantime, the synchronous fluorescence intensities of the mixture solution (for Tf) were measured at $\Delta\lambda$ = 60 nm and $\Delta\lambda$ = 15 nm, respectively.

4. Conclusions

Primuletin (5-hydroxyflavone) forms under the selected working conditions four new complexes with Sm(III), Eu(III), Gd(III), Tb(III) ions. These complexes have been characterized by elemental analysis, thermal analysis (TG, DTA), conductometric measurements and several spectroscopic techniques (FT-IR, UV-Vis, EPR, mass spectra). From the experimental data, the composition and structure, as well as the non-electrolytic nature of the complexes have been established. In the hydroxo complexes obtained, two deprotonated molecules of ligand are bound to the metal ion in a bidentate chelate manner. The ligand and its Ln(III) complexes exhibit strong interaction with DNA, and Ln(III) complexes have much stronger DNA binding affinities than the ligand. Furthermore, the four new complexes and the ligand interacted with HSA and transferrin have been carried out and the apparent association constants (K_a) and thermodynamic parameters (ΔH, ΔS, ΔG) have been calculated at 299 K, 308 K, and 318 K. The binding propensity varies with the binding propensity varying in the following order: (**3**) < (**1**) < (**2**) < (**4**) < 5-HOF (HSA); 5-HOF < (**3**) < (**1**)< (**4**) < (**2**) (Tf). These new lanthanide complexes show promising preliminary results, which may prove useful for the future studies. We can assume that these new complexes may be efficient tools for the in vitro study of molecular mechanisms underlying tumour development or as anticancer drugs.

Supplementary Materials: Supplementary materials can be accessed at: http://www.mdpi.com/1420-3049/21/12/1737/s1.

Acknowledgments: The authors thank the Carol Davila University of Medicine and Pharmacy from Bucharest for the financial support.

Author Contributions: For this research article the authors have contributed in the following way: Valentina Uivarosi proposed the idea for the synthesis of the complexes and the interactions with biomacromolecules contributed to the study's design and supervised the entire project; Alexandra-Cristina Munteanu carried out the field work, processed the data, and wrote large sections of the paper; Mihaela Badea and Rodica Olar performed the thermogravimetric analysis and registered the UV-Vis spectra; Luigi Silvestro and Constanta Dulea performed the mass spectroscopy studies; Constantin-Daniel Negut performed the EPR studies. All authors provided essential information in the interpretation of the results and contributed to the writing of the paper.

Conflicts of Interest: The authors declare no conflict of interest.

References

1. Selvaraj, S.; Krishnaswamy, S.; Devashya, V.; Sethuraman, S.; Krishnan, U.M. Flavonoid-metal ion complexes: A novel class of therapeutic agents. *Med. Res. Rev.* **2014**, *34*, 677–702. [CrossRef] [PubMed]
2. Arun, T.R.; Subramanian, R.; Packianathan, S.; Raman, N. Fluorescence Titrations of Bio-relevant Complexes with DNA: Synthesis, Structural Investigation, DNA Binding/Cleavage, Antimicrobial and Molecular Docking Studies. *J. Fluoresc.* **2015**, *25*, 1127–1140. [CrossRef] [PubMed]
3. Marinic, M.; Piantanida, I.; Rusak, G.; Zinic, M. Interactions of quercetin and its lanthane complex with double stranded DNA/RNA and single stranded RNA: Spectrophotometric sensing of poly G. *J. Inorg. Biochem.* **2006**, *100*, 288–298. [CrossRef] [PubMed]
4. Li, J.; Kang, J.; Lu, J.; Li, X.; Tang, J.; Zhang, H.; Zhang, Y. Determination of calf thymus DNA using resonance light-scattering quenching method based on the terbium(III) (Tb^{3+})/europium(III) (Eu^{3+})–Quercetin system. *J. Lumin.* **2009**, *129*, 906–911. [CrossRef]
5. Liu, J.Y.; Ren, N.; Zhang, J.J.; Zhang, C.Y.; Song, H.H. Crystal structures, thermal behavior and biological activities of lanthanide compounds with 2,4-dichlorobenzoic acid and 1,10-phenanthroline. *Ind. Eng. Chem. Res.* **2013**, *52*, 6156–6163. [CrossRef]

6. Wang, Q.; Huang, M.; Huang, Y.; Zhang, J.S.; Zhou, G.F.; Zeng, R.Q.; Yang, X.B. Synthesis, characterization, DNA interaction, and antitumor activities of mixed-ligand metal complexes of kaempferol and 1,10-phenanthroline/2,20-bipyridine. *Med. Chem. Res.* **2014**, *23*, 2659–2666. [CrossRef]
7. Kopacz, M.; Woźnicka, E.; Gruszecka, J. Antibacterial activity of morin and its complexes with La(III), Gd(III) and Lu(III) ions. *Acta Pol. Pharm. Drug Res.* **2005**, *62*, 65–67.
8. Xu, W.; Zhou, Y.; Huang, D.; Su, M.; Wang, K.; Hong, M. A highly sensitive and selective fluorescent sensor for detection of Al(3+) using a europium(III) quinolinecarboxylate. *Inorg. Chem.* **2014**, *53*, 6497–6499. [CrossRef] [PubMed]
9. Pusz, J.; Woznicka, E.; Wolowiec, S.; Umbreit, M.H. New solid compounds of Tb(III), Ho(III), Er(III) and Yb(III) with chrysin. *J. Therm. Anal. Calorim.* **2009**, *97*, 987–992. [CrossRef]
10. Ansari, A.A. DFT and ^{1}H-NMR molecular spectroscopic studies on biologically anti-oxidant active paramagnetic lanthanide(III)-chrysin complexes. *Main Group Chem.* **2008**, *7*, 43–56. [CrossRef]
11. Pusz, J.; Wolowiec, S. Solid compounds of Ce(III), Pr(III), Nd(III), and Sm(III) ions with chrysin. *J. Therm. Anal. Calorim.* **2012**, *110*, 813–821. [CrossRef]
12. Ansari, A.A. ^{1}H-NMR, spectroscopic and molecular modeling studies on paramagnetic lanthanide(III)-quercetin complexes. *Main Group Chem.* **2008**, *7*, 15–30. [CrossRef]
13. Ansari, A.A. Paramagnetic NMR shift, spectroscopic and molecular modeling studies of lanthanide(III)-morin complexes. *J. Coord. Chem.* **2008**, *61*, 3869–3878. [CrossRef]
14. Nowak, D.; Woznicka, E.; Kuzniar, A.; Kopacz, M. Magnetism of the lanthanides(III) complexes with some polihydroxyflavones. *J. Alloys Compd.* **2006**, *425*, 59–63. [CrossRef]
15. Woznicka, E.; Kopacz, M.; Umbreit, M.; Klos, J. New complexes of La(III), Ce(III), Pr(III), Nd(III), Sm(III), Eu(III) and Gd(III) ions with morin. *J. Inorg. Biochem.* **2007**, *101*, 774–782. [CrossRef] [PubMed]
16. Rescifina, A.; Zagni, C.; Varrica, M.G.; Pistarà, V.; Corsaro, A. Recent advances in small organic molecules as DNA intercalating agents: Synthesis, activity, and modeling. *Eur. J. Med. Chem.* **2013**, *74*, 95–115. [CrossRef] [PubMed]
17. Dolatabadi, J.E.N. Molecular aspects on the interaction of quercetin and its metal complexes with DNA. *Int. J. Biol. Macromol.* **2011**, *48*, 227–233. [CrossRef] [PubMed]
18. Liu, Z.; Liu, S.; Wang, X.; Li, P.; He, Y. A novel quantum dots-based OFF–ON fluorescent biosensor for highly selective and sensitive detection of double-strand DNA. *Sens. Actuators B Chem.* **2013**, *176*, 1147–1153. [CrossRef]
19. Zhang, G.; Guo, J.; Pan, J.; Chen, X.; Wang, J. Spectroscopic studies on the interaction of morin-Eu(III) complex with calf thymus DNA. *J. Mol. Struct.* **2009**, *923*, 114–119. [CrossRef]
20. Li, Z.; Kang, J.; Lu, X. Electrochemical study on behavior of $EuMo_2$ complex and its interaction with DNA. *Nucleosides Nucleotides Nucleic Acids* **2007**, *26*, 9–22. [CrossRef] [PubMed]
21. Wang, B.D.; Yang, Z.Y.; Wang, Q.; Cai, T.K.; Crewdson, P. Synthesis, characterization, cytotoxic activities, and DNA-binding properties of the La(III) complex with Naringenin Schiff-base. *Bioorg. Med. Chem.* **2006**, *14*, 1880–1888. [CrossRef] [PubMed]
22. Yin, B.T.; Yan, C.Y.; Peng, X.M.; Zhang, S.L.; Rasheed, S.; Geng, R.X.; Zhou, C.H. Synthesis and biological evaluation of α-triazolyl chalcones as a new type of potential antimicrobial agents and their interaction with calf thymus DNA and human serum albumin. *Eur. J. Med. Chem.* **2014**, *71*, 148–159. [CrossRef] [PubMed]
23. Martínez, A.; Suárez, J.; Shand, T.; Magliozzo, R.S.; Sánchez-Delgado, R.A. Interactions of arene-Ru(II)-chloroquine complexes of known antimalarial and antitumor activity with human serum albumin (HSA) and transferrin. *J. Inorg. Biochem.* **2011**, *105*, 39–45. [CrossRef] [PubMed]
24. Zhang, X.F.; Han, R.M.; Sun, X.R.; Li, G.Y.; Yang, Q.F.; Li, Q.; Gai, W.; Zhang, M.; Chen, L.; Yang, G.; et al. The effect of the skeleton structure of flavanone and flavonoid on interaction with transferrin. *Bioorg. Med. Chem. Lett.* **2013**, *23*, 6677–6681. [CrossRef] [PubMed]
25. Valant-Vetschera, K.M.; Bhutia, T.D.; Wollenweber, E. Exudate flavonoids of *Primula* spp: Structural and biogenetic chemodiversity. *Nat. Prod. Commun.* **2009**, *4*, 365–370. [PubMed]
26. Valant-Vetschera, K.M.; Bhutia, T.D.; Wollenweber, E. Chemodiversity of exudate flavonoids in *Dionysia* (*Primulaceae*): A comparative study. *Phytochemistry* **2010**, *71*, 937–947. [CrossRef] [PubMed]
27. Calderone, V.; Chericoni, S.; Martinelli, C.; Testai, L.; Nardi, A.; Morelli, I.; Breschi, M.C.; Martinotti, E. Vasorelaxing effects of flavonoids: Investigation on the possible involvement of potassium channels. *Naunyn Schmiedebergs Arch. Pharmacol.* **2004**, *370*, 290–298. [CrossRef] [PubMed]

28. Nishizaki, Y.; Ishimoto, Y.; Hotta, Y.; Hosoda, A.; Yoshikawa, H.; Akamatsu, M.; Tamura, H. Effect of flavonoids on androgen and glucocorticoid receptors based on in vitro reporter gene assay. *Bioorg. Med. Chem. Lett.* **2009**, *19*, 4706–4710. [CrossRef] [PubMed]
29. Dangleterre, L.; Cornard, J.-P.; Lapouge, C. Spectroscopic and theoretical investigation of the solvent effects on Al(III)–hydroxyflavone complexes. *Polyhedron* **2008**, *27*, 1581–1590. [CrossRef]
30. Sarowar, C.H.; Moran, G.; Willett, G.D. A study of divalent metal cations Cu^{2+}, Zn^{2+} and Pb^{2+} attachment to 3-hydroxyflavone, 5-hydroxyflavone and 5-methoxyflavone by nanoelectrospray ionization LTQ Orbitrap mass spectrometry. *Int. J. Mass Spectrom.* **2013**, *333*, 44–54. [CrossRef]
31. Cornard, J.P.; Merlin, J.C. Structural and spectroscopic investigation of 5-hydroxyflavone and its complex with aluminium. *J. Mol. Struct.* **2001**, *569*, 129–138. [CrossRef]
32. Jabeen, E.; Ahmed, S.; Murtaza, I.; Ali, T.; Hameed, S. Radical scavenging propensity of Cu^{2+}, Fe^{3+} complexes of flavonoids and in vivo radical scavenging by Fe^{3+}-primuletin. *Spectrochim. Acta A* **2017**, *171*, 432–438. [CrossRef] [PubMed]
33. Sathish, R.S.; Goutam, A.R.; Rao, G.N.; Janardhana, C. A fluorescent fluoride ion probe based on a self-organized ensemble of 5-hydroxyflavone-Al(III) complex. *Spectrochim. Acta A* **2008**, *69*, 282–285. [CrossRef] [PubMed]
34. Yuji, H.; Sano, T.; Fujii, H.; Nishio, Y.; Takanashi, H.; Shibata, K.H. Organic light emitting diodes using 3- or 5-hydroxyflavone–metal complexes. *Appl. Phys. Lett.* **1997**, *71*, 3338–3340.
35. Uivarosi, V.; Barbuceanu, S.F.; Aldea, V.; Arama, C.C.; Badea, M.; Olar, R.; Marinescu, D. Synthesis, Spectral and Thermal Studies of New Rutin Vanadyl Complexes. *Molecules* **2010**, *15*, 1578–1589. [CrossRef] [PubMed]
36. Uivarosi, V.; Badea, M.; Olar, R.; Draghici, C.; Barbuceanu, S.F. Synthesis and Characterization of Some New Complexes of Magnesium (II) and Zinc (II) with the Natural Flavonoid Primuletin. *Molecules* **2013**, *18*, 7631–7645. [CrossRef] [PubMed]
37. Vijayaraghavan, K.; Iyyam Pillai, S.; Subramanian, S.P. Design, synthesis and characterization of zinc-3 hydroxy flavone, a novel zinc metallo complex for the treatment of experimental diabetes in rats. *Eur. J. Pharmacol.* **2012**, *680*, 122–129. [CrossRef] [PubMed]
38. Iyyam Pillai, S.; Subramanian, S.P.; Kandaswamy, M.A. Novel insulin mimetic vanadium flavonol complex: Synthesis, characterization and in vivo evaluation in STZ-induced rats. *Eur. J. Med. Chem.* **2013**, *63*, 109–117. [CrossRef] [PubMed]
39. De Souza, R.F.V.; De Giovani, W.F. Synthesis, spectral and electrochemical properties of Al(III) and Zn(II) complexes with flavonoids. *Spectrochim. Acta A* **2005**, *61*, 1985–1990. [CrossRef] [PubMed]
40. Sastri, V.S.; Bünzli, J.C.; Rao, V.R.; Rayudu, G.V.S.; Perumareddi, J.R. Spectroscopy of Lanthanide Complexes. In *Modern Aspects of Rare Earths and Their Complexes*; Sastri, V.S., Bünzli, J.C., Rao, V.R., Rayudu, G.V.S., Perumareddi, J.R., Eds.; Elsevier: Amsterdam, The Netherlands, 2003; p. 619.
41. Henmi, K.; Hinatsu, Y.; Masaki, N.M. Crystal Structures and Magnetic Properties of Ordered Perovskites Ba_2LnNbO_6 (*Ln*=Lanthanide Elements). *J. Solid State Chem.* **1999**, *148*, 353–360. [CrossRef]
42. Szyczewski, A.; Lis, S.; Krzystek, J.; Staninski, K.; Klonkowski, A.; Kruczynski, Z.; Pietraszkiewicz, M. Gadolinium(III) cryptates investigated by multifrequency EPR. *J. Alloys Compd.* **2008**, *451*, 182–185. [CrossRef]
43. Gudasi, K.B.; Shenoy, R.V.; Vadavi, R.S.; Patil, M.S.; Patil, S.A.; Hanchinal, R.R.; Desai, S.A.; Lohithaswa, H. Lanthanide(III) and Yttrium(III) Complexes of Benzimidazole-2-Acetic Acid: Synthesis, Characterisation and Effect of La(III) Complex on Germination of Wheat. *Bioinorg. Chem. Appl.* **2006**, *2006*, 75612. [CrossRef] [PubMed]
44. Mazur, M.; Poprac, P.; Valko, M.; Rhodes, C. 'U-spectrum' type of Gd(III) EPR spectra recorded at various stages of TEOS-based sol-gel process. *J. Sol-Gel Sci. Technol.* **2016**, *79*, 220–227. [CrossRef]
45. Essawy, A.A.; Afifi, M.A.; Moustafa, H.; El-Medani, S.M. DFT calculations, spectroscopic, thermal analysis and biological activity of Sm(III) and Tb(III) complexes with 2-aminobenzoic and 2-amino-5-chloro-benzoic acids. *Spectrochim. Acta A* **2014**, *131*, 388–397. [CrossRef] [PubMed]
46. Tan, J.; Wang, B.; Zhu, L. DNA binding and oxidative DNA damage induced by a quercetin copper (II) complex. *J. Biol. Inorg. Chem.* **2009**, *14*, 727–739. [CrossRef] [PubMed]
47. Rusak, G.; Piantanida, I.; Masic, L.; Kapuralin, K.; Durgo, K.; Kopjar, N. Spectrophotometric analysis of flavonoids-DNA interactions and DNA damaging/protecting and cytotoxic potential of flavonoids in human peripheral blood lymphocytes. *Chem. Biol. Interact.* **2010**, *188*, 181–189. [CrossRef] [PubMed]

48. Buchtík, R.; Trávníček, Z.; Vančo, J.; Herchel, R.; Dvořák, Z. Synthesis, characterization, DNA interaction and cleavage, and in vitro cytotoxicity of copper(II) mixed-ligand complexes with 2-phenyl-3-hydroxy-4(1H)-quinolinone. *Dalton Trans.* **2011**, *40*, 9404–9412. [CrossRef] [PubMed]
49. Navarra, M.; Hernandez, C.; Colmenares, I.; Hernandez, P.; Fernandez, M.; Sierraalta, A.; Marchan, E. Synthesis and characterization of $[Au(dppz)_2]Cl_3$. DNA interaction studies and biological activity against *Leishmania(L) mexicana*. *J. Inorg. Biochem.* **2007**, *101*, 111–116. [CrossRef] [PubMed]
50. Lakowicz, J.R.; Weber, G. Quenching of fluorescence by oxygen. Probe for structural fluctuations in macromolecules. *Biochemistry* **1973**, *12*, 4161–4170. [CrossRef] [PubMed]
51. Sarzehi, S.; Chamani, J. Investigation on the interaction between tamoxifen and human holo-transferrin: Determination of the binding mechanism by fluorescence quenching, resonance light scattering and circular dichroism methods. *Int. J. Biol. Macromol.* **2010**, *47*, 558–569. [CrossRef] [PubMed]
52. Varlan, A.; Hillebrand, M. Bovine and Human Serum Albumin Interactions with 3-Carboxyphenoxathiin Studied by Fluorescence and Circular Dichroism Spectroscopy. *Molecules* **2010**, *15*, 3905–3919. [CrossRef] [PubMed]
53. Wu, S.; Yuan, W.; Wang, H.; Zhang, Q.; Liu, M.; Yu, K. Synthesis, crystal structure and interaction with DNA and HSA of (*N*,*N*′-dibenzylethane-1,2-diamine) transition metal complexes. *J. Inorg. Biochem.* **2008**, *102*, 2026–2034. [CrossRef] [PubMed]
54. Du, H.; Xiang, J.; Zhang, Y.; Tang, Y. A spectroscopic and molecular modeling study of sinomenine binding to transferrin. *Bioorg. Med. Chem. Lett.* **2007**, *17*, 1701–1704. [CrossRef] [PubMed]
55. Fu, X.B.; Lin, Z.H.; Liu, H.F.; Le, X.Y. A new ternary copper(II) complex derived from 2-(2′-pyridyl)benzimidazole and glycylglycine: Synthesis, characterization, DNA binding and cleavage, antioxidation and HSA interaction. *Spectrochim. Acta A* **2014**, *122*, 22–33. [CrossRef] [PubMed]
56. Zhang, X.F.; Yang, G.; Dong, Y.; Zhao, Y.Q.; Sun, X.R.; Chen, L.; Chen, H.B. Studies on the binding of fulvic acid with transferrin by spectroscopic analysis. *Spectrochim. Acta A* **2015**, *137*, 1280–1285. [CrossRef] [PubMed]
57. Gao, Y.; Shao, C.; Ji, W.; Xiao, M.; Yi, F.; Zhou, T.; Zi, Y. Studies on the Binding Mechanism of VB1 and VB9 with Trypsin. *Am. J. Anal. Chem.* **2013**, *4*, 771–775. [CrossRef]
58. Frisch, M.J.; Trucks, G.W.; Schlegel, H.B.; Scuseria, G.E.; Robb, M.A.; Cheeseman, J.R.; Scalmani, G.; Barone, V.; Mennucci, B.; Petersson, G.A.; et al. *Gaussian 09, Revision A.02*; Gaussian: Wallingford, CT, USA, 2009.
59. Dolg, M.; Stoll, H.; Savin, A.; Preuss, H. Energy-adjusted pseudopotentials for the rare earth elements. *Theor. Chem. Acc.* **1989**, *75*, 173–194. [CrossRef]
60. Alkauskas, A.; Baratoff, A.; Bruder, C. Gaussian Form of Effective Core Potential and Response Function Basis Set Derived from Troullier–Martins Pseudopotential: Results for Ag and Au. *J. Phys. Chem. A* **2004**, *108*, 6863–6868. [CrossRef]
61. Georgieva, I.; Mihaylov, T.; Trendafilova, N. Lanthanide and transition metal complexes of bioactive coumarins: Molecular modeling and spectroscopic studies. *J. Inorg. Biochem.* **2014**, *135*, 100–112. [CrossRef] [PubMed]
62. Mujahid, M.; Kia, A.F.A.; Duff, B.; Egan, D.A.; Devereux, M.; McClean, S.; Walsh, M.; Trendafilova, N.; Georgieva, I.; Creaven, B.S. Spectroscopic studies, DFT calculations, and cytotoxic activity of novel silver(I) complexes of hydroxy *ortho*-substituted-nitro-2 *H*-chromen-2-one ligands and a phenanthroline adduct. *J. Inorg. Biochem.* **2015**, *153*, 103–113. [CrossRef] [PubMed]
63. Aslam, S.; Isab, A.A.; Alotaibi, M.A.; Saleem, M.; Monim-ul-Mehboob, M.; Ahmad, S.; Georgieva, I.; Trendafilova, N. Synthesis, spectroscopic characterization, DFT calculations and antimicrobial properties of silver(I) complexes of 2,2′-bipyridine and 1,10-phenanthroline. *Polyhedron* **2016**, *115*, 212–218. [CrossRef]

Sample Availability: Samples of the compounds (**1**), (**2**), (**3**), (**4**) are available from Valentina Uivarosi.